

Experimental generation of polarization entanglement from spontaneous parametric down-conversion pumped by spatiotemporally highly incoherent light

Cheng Li^{1,*}, Boris Braverman,¹ Girish Kulkarni,¹ and Robert W. Boyd^{1,2,†}

¹*Department of Physics, University of Ottawa, Ottawa, Ontario, Canada K1N 6N5*

²*Institute of Optics, University of Rochester, Rochester, New York 14627, USA*



(Received 31 October 2022; accepted 20 March 2023; published 10 April 2023)

We investigate the cross influence of the pump coherence on the entanglement produced from spontaneous parametric down-conversion (SPDC) in different degrees of freedom (DOFs). We experimentally demonstrate the generation of polarization entanglement from SPDC pumped by a spatiotemporally highly incoherent (STHI) light-emitting diode. Our quantum state tomography measurements using multimode collection fibers to avoid postselection yield a two-qubit state with the concurrence of 0.531 ± 0.006 and purity of 0.647 ± 0.005 , in excellent agreement with our theoretically predicted concurrence of 0.552 and purity of 0.652. We find that using an STHI pump reduces the entanglement and purity of the output polarization two-qubit state due to a coupling between the spatiotemporal and polarization DOFs introduced by the birefringence and dispersion of the nonlinear crystal. The viability of SPDC with STHI pumps is important for two reasons: (i) STHI sources are ubiquitous and available at a wider range of wavelengths than lasers, and (ii) the generated STHI polarization-entangled two-photon states could potentially be useful in long-distance quantum communication schemes due to their robustness to scattering.

DOI: [10.1103/PhysRevA.107.L041701](https://doi.org/10.1103/PhysRevA.107.L041701)

In the last few decades, entangled photon pairs produced from spontaneous parametric down-conversion (SPDC) [1–3] have become a ubiquitous resource for fundamental experiments in quantum optics [4–10] and practical realizations of quantum communication protocols [11–13]. In the context of SPDC, a number of studies have sought to understand the fundamental origin of the nonlocal correlations of the entangled photons, and how those correlations can be precisely tailored for various quantum applications [14–24]. In particular, the influence of the pump field’s coherence properties on the generated two-photon entanglement has been investigated in the spatial [14–19], temporal [20–22], and polarization [23,24] degrees of freedom (DOFs). In each DOF, it was shown that in the absence of postselection, the pump’s coherence sets an upper bound on the generated entanglement in the same DOF. For instance, in the polarization DOF, if the setup is a closed system that does not involve postselection, the pump’s polarization coherence determines the maximum achievable polarization entanglement of the generated two-qubit signal-idler state [23]. However, such studies implicitly ignore or assume perfect pump coherence in every DOF other than the specific DOF under consideration. As a result, the cross influence of the pump coherence in a given DOF on the entanglement generated in a different DOF is not well understood. For instance, it is not well understood if a lack of spatial or temporal coherence in a perfectly polarized pump field would prevent or somehow influence the two-qubit polarization entanglement between the signal and idler photons.

In this context, a theoretical study predicts that polarization entanglement decreases with decreasing pump spatial coherence [25], whereas an experimental study concludes the exact opposite [26]. However, the conclusion of Ref. [26] is dubious because their detection employs single-mode fibers (SMFs) that effectively postselect for a spatially highly coherent pump.

In this Letter, we experimentally investigate the polarization entanglement produced from SPDC pumped by a perfectly polarized spatiotemporally highly incoherent (STHI) beam from a light-emitting diode (LED). In contrast with Ref. [26], we collect the entangled photons using large-aperture multimode fibers (MMFs) to significantly reduce the influence of postselection. The output two-qubit state is measured to have a concurrence of 0.531 ± 0.006 and a purity of 0.647 ± 0.005 , in excellent agreement with our theoretically predicted concurrence of 0.552 and purity of 0.652. In essence, we find that the birefringence and dispersion of the crystal medium couple the spatiotemporal and polarization degrees of freedom in the experiment. Consequently, the lack of spatiotemporal coherence in the pump results in a degradation of the entanglement and purity of the output polarization two-qubit signal-idler state when measured in a nonpostselective manner. In what follows, we describe the theory and then present the experimental results of our quantum state tomography and polarization correlation measurements.

We consider SPDC pumped by spatiotemporally partially coherent light in the type-I double-crystal configuration outlined in Ref. [27]. We define \mathbf{q}_j and ω_j for $j = p, s, i$ as the transverse wave vectors and frequencies corresponding to the pump, signal, and idler, respectively. From conservation of transverse momentum and energy, it follows that $\mathbf{q}_p = \mathbf{q}_s + \mathbf{q}_i$

*cli221@uottawa.ca

†rboyd@uottawa.ca

and $\omega_p = \omega_s + \omega_i$. The state vector describing the far-field spatiotemporal and polarization correlations of a given element in the generated two-photon ensemble can be written as (see Supplemental Material [28])

$$|\psi\rangle = A \iiint d\mathbf{q}_s d\mathbf{q}_i d\omega_s d\omega_i \Phi(\Delta k_z L) \times [E_V(\mathbf{q}_p, \omega_p) |H, \mathbf{q}_s, \omega_s\rangle |H, \mathbf{q}_i, \omega_i\rangle + E_H(\mathbf{q}_p, \omega_p) e^{i\chi(\mathbf{q}_s, \omega_s, \mathbf{q}_i, \omega_i)} |V, \mathbf{q}_s, \omega_s\rangle |V, \mathbf{q}_i, \omega_i\rangle], \quad (1)$$

where A is a normalization factor, Δk_z is the longitudinal wave-vector mismatch, L is the length of each individual crystal, $\Phi(\Delta k_z L) = \text{sinc}[\Delta k_z L/2] e^{i\Delta k_z L/2}$ is the phase-matching function, $E_{H(V)}(\mathbf{q}_p, \omega_p)$ denotes the horizontal (vertical) polarization component of the pump spectral amplitude inside the crystal, and $|H(V), \mathbf{q}_j, \omega_j\rangle$ for $j = s, i$ denotes the basis vector for the horizontal (vertical) polarization of the corresponding spatiotemporal mode of the signal and idler photon, respectively. The quantity $\chi(\mathbf{q}_s, \omega_s, \mathbf{q}_i, \omega_i)$ represents a relative phase acquired due to spatial and temporal walk-off between the two-photon state amplitudes generated in the two crystals. However, we assume that by using temporal and spatial walk-off compensation elements in the setup, one can ensure $\chi(\mathbf{q}_s, \omega_s, \mathbf{q}_i, \omega_i) \approx 0$ (see Supplemental Material [28]). For a pump field with spectral amplitude $E_0(\mathbf{q}_p, \omega_p)$ that is linearly polarized at 45° or -45° before entering the crystal, we have $|E_H(\mathbf{q}_p, \omega_p)| = |E_V(\mathbf{q}_p, \omega_p)| = |E_0(\mathbf{q}_p, \omega_p)|/\sqrt{2}$ and the relative phase between $E_H(\mathbf{q}_p, \omega_p)$ and $E_V(\mathbf{q}_p, \omega_p)$ is 0 or π , respectively. However, inside the crystal, the birefringence and dispersion properties of the medium induce a relative phase $\phi(\mathbf{q}_p, \omega_p)$ between $E_H(\mathbf{q}_p, \omega_p)$ and $E_V(\mathbf{q}_p, \omega_p)$. Using these relations, the final measured polarization two-qubit state ρ can be written in the computational basis $\{|HH\rangle, |HV\rangle, |VH\rangle, |VV\rangle\}$ as

$$\rho = \text{Tr}_{\text{spat, temp}}(\langle |\psi\rangle \langle \psi| \rangle) = \begin{bmatrix} 1/2 & 0 & 0 & \mu/2 \\ 0 & 0 & 0 & 0 \\ 0 & 0 & 0 & 0 \\ \mu^*/2 & 0 & 0 & 1/2 \end{bmatrix}, \quad (2)$$

where $\text{Tr}_{\text{spat, temp}}$ denotes a partial trace over the spatial and temporal degrees of freedom, $\langle \cdot \rangle$ denotes an ensemble average over many realizations of the pump field, and $|A|^2$ is chosen such that $\text{Tr}(\rho) = 1$. The quantity μ is then written as (see Supplemental Material [28])

$$\mu = |A|^2 \int_{\Delta \mathbf{q}_p} d\mathbf{q}_p \int_{\Delta \omega_p} d\omega_p |E_0(\mathbf{q}_p, \omega_p)|^2 e^{i\phi(\mathbf{q}_p, \omega_p)}, \quad (3)$$

where $\Delta \mathbf{q}_p = \Delta \mathbf{q}_s + \Delta \mathbf{q}_i$, and $\Delta \omega_p = \Delta \omega_s + \Delta \omega_i$; $\Delta \mathbf{q}_{s(i)}$ denotes the angular bandwidth corresponding to the detection aperture in the signal (idler) arm, and $\Delta \omega_{s(i)}$ denotes the bandwidth of the spectral filter in the signal (idler) arm. It may be verified that $|\mu|$ satisfies $0 \leq |\mu| \leq 1$, with $|\mu| \rightarrow 0$ when $\phi(\mathbf{q}_p, \omega_p)$ varies rapidly, and $|\mu| \rightarrow 1$ when $\phi(\mathbf{q}_p, \omega_p)$ is constant, in the integration region. Moreover, $|\mu|$ determines the purity $\text{Tr}(\rho^2) = \{1 + |\mu|^2\}/2$ and the concurrence $C(\rho) = |\mu|$ of the measured two-qubit state. In this work, we use concurrence to quantify the entanglement because, in contrast with the Bell-Clauser-Horne-Shimony-Holt

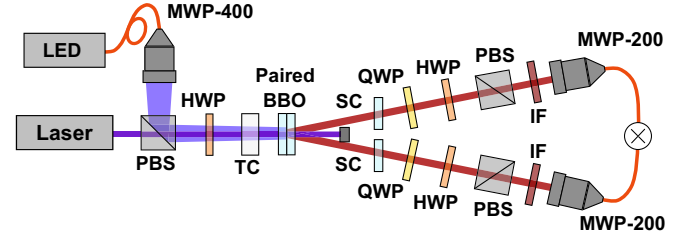


FIG. 1. Schematic diagram of the experimental setup. LED: light-emitting diode; PBS: polarizing beam splitter; HWP: half-wave plate; TC: temporal compensator; BBO: β -barium borate; SC: spatial compensator; QWP: quarter-wave plate; IF: interference filter; MMF-400 (200): multimode fiber with a core diameter of 400 (200) μm .

parameter, which is only a sufficient but not necessary entanglement witness [29], the concurrence can be used to quantify the degree of entanglement of an arbitrary two-qubit state [30].

We now consider the effect of the pump's spatiotemporal coherence on the measured two-qubit state. For a spatiotemporally highly coherent pump such as a laser, the function $E_0(\mathbf{q}_p, \omega_p)$ is highly narrow. Consequently, the averaging of $e^{i\phi(\mathbf{q}_p, \omega_p)}$ in Eq. (3) effectively occurs over a very small integration region, which leads to $|\mu|$ being close to unity, irrespective of $\Delta \mathbf{q}_{s(i)}$ and $\Delta \omega_{s(i)}$. This predicts high measured values of concurrence and purity of two-qubit states produced from a laser pump, regardless of the detection system. However, for an STHI pump such as an LED, the function $E_0(\mathbf{q}_p, \omega_p)$ has support over a broad range of \mathbf{q}_p and ω_p , and, consequently, the role of $\Delta \mathbf{q}_{s(i)}$ and $\Delta \omega_{s(i)}$ in the integrations in Eq. (3) becomes significant. For a detection system that employs SMFs and narrow-band spectral filters, $\Delta \mathbf{q}_{s(i)}$ and $\Delta \omega_{s(i)}$ are small. As a result, the averaging of $e^{i\phi(\mathbf{q}_p, \omega_p)}$ in Eq. (3) again effectively occurs over a small integration region constrained by the relations $\mathbf{q}_p = \mathbf{q}_s + \mathbf{q}_i$ and $\omega_p = \omega_s + \omega_i$. This leads to a high value of $|\mu|$, implying high values of purity and concurrence. In other words, the detection postselection obscures the effect of the pump's lack of coherence. However, for a detection system that employs MMFs and broad-band spectral filters, $\Delta \mathbf{q}_{s(i)}$ and $\Delta \omega_{s(i)}$ are large. Consequently, the averaging of $e^{i\phi(\mathbf{q}_p, \omega_p)}$ in Eq. (3) occurs over a much larger range, and the effect of postselection is significantly reduced. In this case, Eq. (3) would yield a reduced value of $|\mu|$, implying a degradation in the purity and concurrence of the measured state. Thus, our theory predicts that an STHI pump results in a degradation of the entanglement and purity of the output polarization two-qubit state, but to observe this degradation, it is necessary to use MMFs to collect the entangled photons.

In Fig. 1, we depict our experimental setup. The optical field from a Thorlabs M405L3 LED of center wavelength 405 nm, and full width at half maximum (FWHM) bandwidth of 20 nm, is butt-coupled into an MMF with core diameter 400 μm and numerical aperture 0.39, and coupled out into free space using a microscope objective. The LED light at the output of the fiber is measured to be 6 mW. The resulting collimated LED beam is then made linearly polarized at 45° by passing it through a polarizing beam splitter (PBS) and a half-wave plate (HWP), and then made incident onto a paired

β -barium borate (BBO) double crystal cut for noncollinear emission with a half-opening angle of 3° for perpendicular pump incidence. The double crystal consists of two identically cut 0.5-mm-thick type-I BBO crystals attached to each other with their optic axes oriented perpendicularly to one another. An ultraviolet continuous-wave laser with center wavelength 405 nm, bandwidth 2 nm, and power 20 mW is made linearly polarized at -45° and aligned as a pump for benchmarking purposes such that experiments performed with the LED pump can be compared with those performed with the laser pump for the same setup. In both cases, the pump photons are propagated through a 5-mm temporal compensation (TC) quartz crystal to precompensate for the temporal walk-off that the two orthogonal polarizations subsequently experience inside the double crystal [31,32]. The conjugate signal and idler photons from two diametrically opposite regions of the noncollinear emission ring are each sent through a 0.25-mm-thick BBO spatial compensation (SC) crystal to compensate for spatial walk-off effects that the photons have experienced inside the double crystal [33]. The photons are then passed through combinations of a quarter-wave plate (QWP), HWP, and PBS to measure their joint two-photon state. Note that we choose all the waveplates in the setup to be zero order and the optics axes of all the waveplates are carefully aligned before taking measurements. This ensures that our results are not influenced by spectral dispersion or manufacturing imperfections of the waveplates. The diameters of waveplates are chosen to be much larger than the beam size to avoid post-selection. The photons are sent through bandpass filters with center wavelength 810 nm and FWHM bandwidth of 10 nm. Subsequently, the photons are coupled into MMFs with core diameter 200 μm and numerical aperture 0.39 placed in the far field. Finally, the photons from the MMFs are detected using PerkinElmer SPCM-QRH-14-FC avalanche photodiodes and their coincidence count rates are extracted using the Universal Quantum Devices (UQD) Logic-16 data-acquisition unit with a coincidence time resolution window of one nanosecond.

We record coincidence rates for different rotation angles of the QWP and HWP in each arm, both for performing quantum state tomography (QST) of the two-photon polarization state and for measuring polarization correlation fringes in mutually unbiased bases. For the former purpose of QST, we record the coincidence rates with 16 different projective measurements, subtract the theoretical accidental count rates, and use the maximum likelihood state estimation (MLSE) algorithm outlined in Ref. [34] to infer the two-qubit density matrix ρ . We then calculate the concurrence $C(\rho)$ [30] and purity $\text{Tr}[\rho^2]$. For the latter purpose of recording polarization correlation fringes, we fix the polarization in the signal arm and record the coincidence rate as a function of the linear polarization in the idler arm, which is defined by an angle θ with respect to the H polarization. For laser-pumped SPDC, we set an acquisition time of 10 s for each basis and the maximum coincidence rate is $\sim 700 \text{ s}^{-1}$. In contrast, for LED-pumped SPDC, we set an acquisition time of 60 min per basis, and the maximum coincidence rate was $\sim 0.04 \text{ s}^{-1}$. Thus, the coincidence rate for LED-pumped SPDC is much smaller than that of laser-pumped SPDC, which could perhaps be explained by the following two reasons: (i) the LED has a lower power than the laser and (ii) the down-conversion efficiency for the LED

pump could be lower than that for the laser pump due to the lack of coherent phase matching [35].

In Fig. 2(a), we depict the theoretically computed relative phase $\phi(\mathbf{q}_p, \omega_p)$. Since the relative phase has only negligible dependence on the wavelength of the pump (see Supplemental Material [28]), we mainly focus on the dependence on the pump transverse wave vector and depict only the relative phase $\phi(\mathbf{q}_p, \omega_{p0} = 2\pi c/\lambda_{p0})$ for the central pump wavelength $\lambda_{p0} = 405 \text{ nm}$. Figures 2(b) and 2(c) depict the theoretically predicted and experimentally measured two-photon density matrices for laser- and LED-pumped SPDC, respectively. For laser-pumped SPDC, the experimentally measured two-qubit state has a concurrence of 0.955 ± 0.003 and purity of 0.957 ± 0.003 , in close agreement with the theoretically predicted concurrence 0.999 and purity 0.999. We verify that these results are highly stable over multiple measurements performed at different times. For LED-pumped SPDC, the experimentally measured two-qubit state has a concurrence of 0.531 ± 0.006 and purity of 0.647 ± 0.005 , in close agreement with the theoretically predicted concurrence of 0.552 and purity of 0.652. The fidelity of the experimentally measured density matrices to the theoretically predicted ones for laser-pumped and LED-pumped SPDC is 96.07% and 94.92%, respectively.

In Fig. 3, we depict the polarization correlation fringes in horizontal-vertical (H-V) and antidiagonal-diagonal (A-D) bases. Figures 3(a) and 3(b) depict the case of laser-pumped SPDC, whereas Figs. 3(c) and 3(d) depict the case of LED-pumped SPDC. The scatter plots and solid lines represent the experimentally measured data points and the theoretically predicted correlation fringes, respectively. We notice that for laser-pumped SPDC, the fringes in Figs. 3(a) and 3(b) exhibit high contrast in the H-V and A-D bases simultaneously. For quantitative characterization, we calculate the experimental fringe visibility values from sinusoidal fit curves of the measured counts. The fringe visibility in the H-V basis is $98.8 \pm 1.2\%$ and the visibility in the A-D basis is $93.7 \pm 1.8\%$. This presence of strong correlations in two mutually unbiased bases is the characteristic feature of entanglement. In contrast, for LED-pumped SPDC, the fringes in Fig. 3(c) corresponding to the H-V basis exhibit high contrast, but the fringes in Fig. 3(d) exhibit diminished contrast. In particular, the fringe visibility in the H-V basis is $95.9 \pm 6.7\%$, but the fringe visibility in the A-D basis is $39.4 \pm 3.9\%$. In other words, the polarization correlations in the H-V basis remain high, but those in the A-D basis are degraded, which is consistent with the entanglement reduction observed in our QST measurements.

In summary, we experimentally demonstrated the generation of polarization entanglement from SPDC pumped by an STHI LED source. We first presented a theoretical analysis that shows how the birefringence and dispersion of the crystal medium couple the spatiotemporal and polarization degrees of freedom in the experiment. This analysis predicts a degradation in the purity and entanglement of the two-qubit state produced from an STHI LED pump compared to that produced from a coherent laser pump. We then performed the experiment, both with an STHI LED pump and with a laser pump on the same setup for benchmarking purposes. In both cases, we showed that our experimental measurements of the two-qubit state using MMFs to reduce

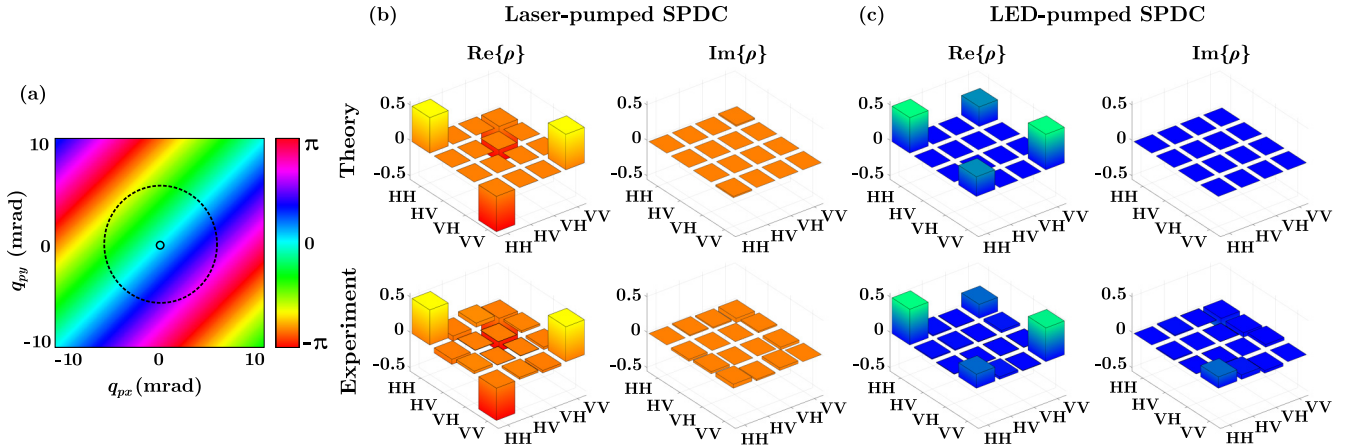


FIG. 2. (a) Theoretical two-dimensional (2D) color plot of $\phi(\mathbf{q}_p, \omega_{p0} = 2\pi c/\lambda_{p0})$ for β -barium borate (BBO), where $\lambda_{p0} = 405$ nm. The solid and dashed circles indicate the effective angular bandwidths of laser and LED pumps, respectively. (b),(c) The theoretically predicted and experimentally measured density matrices for laser-pumped and LED-pumped SPDC, respectively. Note that the laser pump and the LED pump at the PBS output are linearly polarized at -45° and 45° , respectively, because they are coupled into the crystal from different ports of the PBS as shown in Fig. 1.

the influence of postselection are in excellent agreement with our theoretical predictions. For laser-pumped SPDC, the output two-qubit state has a concurrence of 0.955 ± 0.003 and purity of 0.957 ± 0.003 , whereas for LED-pumped SPDC, the two-qubit state has a concurrence of 0.531 ± 0.006 and a purity of 0.647 ± 0.005 . Thus, the entanglement and purity of the polarization-entangled signal-idler state are lower for LED-pumped SPDC compared to laser-pumped SPDC. We also argue that setup instabilities cannot be the primary cause of this reduction because other studies employing highly efficient, periodically poled crystals demonstrate that detection using SMFs yields high purity and entanglement despite the long acquisition times [36]. We were unable to perform such

measurements using SMFs ourselves because of the poor efficiency of our bulk-crystal-based SPDC setup.

In the future, our work might inspire further studies on SPDC with STHI sources. For instance, it may be possible to compensate for $\phi(\mathbf{q}_p, \omega_p)$ and enhance the polarization entanglement produced from a spatiotemporally incoherent pump. Moreover, the analysis in our study is restricted to type-I double-crystal SPDC, which employs critical phase matching. However, there are also noncritical phase-matching methods that do not rely on birefringence, and therefore do not couple the spatial and polarization degrees of freedom [3,37–40]. Using such methods, it may be possible to generate polarization two-qubit states with higher purity and entanglement with an STHI pump. Regardless, our study demonstrates the viability of using SPDC pumped by STHI sources for producing STHI polarization-entangled two-qubit states, which could have two important implications. First, STHI sources such as LEDs and sunlight are ubiquitous and available at a wider range of wavelengths than their coherent counterparts such as lasers. Second, the STHI polarization-entangled two-qubit states produced from SPDC pumped by STHI sources might be well suited for long-distance quantum communication schemes due to their robustness to scattering and turbulence [41–43].

Note added. Recently, we became aware of a similar study being simultaneously carried out by Zhang and co-workers [36]. We believe that our studies complement each other.

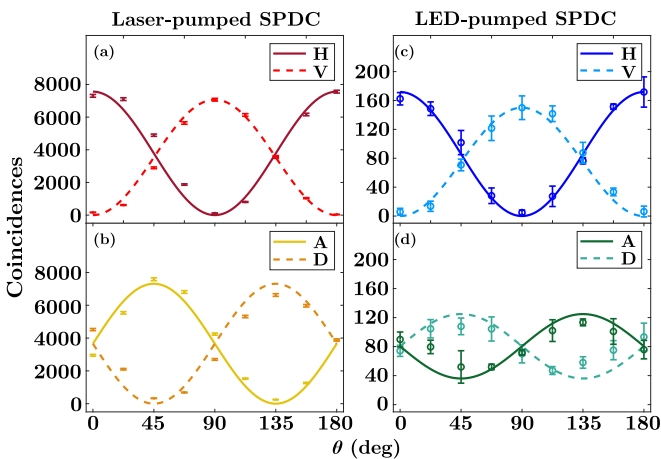


FIG. 3. Polarization correlation fringes in horizontal-vertical (H-V) basis and antidiagonal-diagonal (A-D) basis measured by fixing the signal photon's polarization and varying the idler photon's polarization represented by an angle θ with respect to the horizontal polarization. (a) and (b) correspond to laser-pumped SPDC, whereas (c) and (d) correspond to LED-pumped SPDC. The scatter plots represent the experimentally measured coincidence counts. The solid lines represent the theoretically predicted correlation fringes.

We acknowledge useful discussions with W. Zhang, E. Giese, J. Upham, J. Rioux, and S. Lemieux. We also acknowledge funding from the Canada First Research Excellence Fund (Transformative Quantum Technologies). B.B. acknowledges support from the Banting Postdoctoral Fellowship. R.W.B. acknowledges support through the Natural Sciences and Engineering Research Council (NSERC) of Canada, the Canada Research Chairs program, by U.S. DARPA Award No. W911NF-18-1-0369, U.S. ARO Award No. W911NF-

18-1-0337, U.S. Office of Naval Research MURI Award No. N00014-20-1-2558, U.S. National Science Foundation Award

No. 2138174, and the U.S. Department of Energy Award No. FWP 76295.

-
- [1] D. C. Burnham and D. L. Weinberg, Observation of Simultaneity in Parametric Production of Optical Photon Pairs, *Phys. Rev. Lett.* **25**, 84 (1970).
- [2] C. K. Hong and L. Mandel, Theory of parametric frequency down conversion of light, *Phys. Rev. A* **31**, 2409 (1985).
- [3] R. W. Boyd, *Nonlinear Optics* (Academic Press, San Diego, CA, 2020).
- [4] C. K. Hong, Z. Y. Ou, and L. Mandel, Measurement of Subpicosecond Time Intervals between Two Photons by Interference, *Phys. Rev. Lett.* **59**, 2044 (1987).
- [5] Z. Y. Ou and L. Mandel, Violation of Bell's Inequality and Classical Probability in a Two-Photon Correlation Experiment, *Phys. Rev. Lett.* **61**, 50 (1988).
- [6] G. Weihs, T. Jennewein, C. Simon, H. Weinfurter, and A. Zeilinger, Violation of Bell's Inequality under Strict Einstein Locality Conditions, *Phys. Rev. Lett.* **81**, 5039 (1998).
- [7] Y. H. Shih and C. O. Alley, New Type of Einstein-Podolsky-Rosen-Bohm Experiment Using Pairs of Light Quanta Produced by Optical Parametric Down Conversion, *Phys. Rev. Lett.* **61**, 2921 (1988).
- [8] T. E. Kiess, Y. H. Shih, A. V. Sergienko, and C. O. Alley, Einstein-Podolsky-Rosen-Bohm Experiment Using Pairs of Light Quanta Produced by Type-II Parametric Down-Conversion, *Phys. Rev. Lett.* **71**, 3893 (1993).
- [9] L. J. Wang, X. Y. Zou, and L. Mandel, Induced coherence without induced emission, *Phys. Rev. A* **44**, 4614 (1991).
- [10] X. Y. Zou, L. J. Wang, and L. Mandel, Induced Coherence and Indistinguishability in Optical Interference, *Phys. Rev. Lett.* **67**, 318 (1991).
- [11] R. Ursin, F. Tiefenbacher, T. Schmitt-Manderbach, H. Weier, T. Scheidl, M. Lindenthal, B. Blauensteiner, T. Jennewein, J. Perdigues, P. Trojek, B. Ömer, M. Fürst, M. Meyenburg, J. Rarity, Z. Sodnik, C. Barbieri, H. Weinfurter, and A. Zeilinger, Entanglement-based quantum communication over 144 km, *Nat. Phys.* **3**, 481 (2007).
- [12] J. Yin, Y.-H. Li, S.-K. Liao, M. Yang, Y. Cao, L. Zhang, J.-G. Ren, W.-Q. Cai, W.-Y. Liu, S.-L. Li, R. Shu, Y.-M. Huang, L. Deng, L. Li, Q. Zhang, N.-L. Liu, Y.-A. Chen, C.-Y. Lu, X.-B. Wang, F. Xu *et al.*, Entanglement-based secure quantum cryptography over 1120 kilometres, *Nature (London)* **582**, 501 (2020).
- [13] D. Bouwmeester, J.-W. Pan, K. Mattle, M. Eibl, H. Weinfurter, and A. Zeilinger, Experimental quantum teleportation, *Nature (London)* **390**, 575 (1997).
- [14] A. K. Jha and R. W. Boyd, Spatial two-photon coherence of the entangled field produced by down-conversion using a partially spatially coherent pump beam, *Phys. Rev. A* **81**, 013828 (2010).
- [15] E. Giese, R. Fickler, W. Zhang, L. Chen, and R. W. Boyd, Influence of pump coherence on the quantum properties of spontaneous parametric down-conversion, *Phys. Scr.* **93**, 084001 (2018).
- [16] C. H. Monken, P. H. Souto Ribeiro, and S. Pádua, Transfer of angular spectrum and image formation in spontaneous parametric down-conversion, *Phys. Rev. A* **57**, 3123 (1998).
- [17] H. Defienne and S. Gigan, Spatially entangled photon-pair generation using a partial spatially coherent pump beam, *Phys. Rev. A* **99**, 053831 (2019).
- [18] W. Zhang, R. Fickler, E. Giese, L. Chen, and R. W. Boyd, Influence of pump coherence on the generation of position-momentum entanglement in optical parametric down-conversion, *Opt. Express* **27**, 20745 (2019).
- [19] L. Hutter, G. Lima, and S. P. Walborn, Boosting Entanglement Generation in Down-Conversion with Incoherent Illumination, *Phys. Rev. Lett.* **125**, 193602 (2020).
- [20] A. V. Burlakov, M. V. Chekhova, O. A. Karabutova, and S. P. Kulik, Biphoton interference with a multimode pump, *Phys. Rev. A* **63**, 053801 (2001).
- [21] A. K. Jha, M. N. O'Sullivan, Kam Wai Clifford Chan, and R. W. Boyd, Temporal coherence and indistinguishability in two-photon interference effects, *Phys. Rev. A* **77**, 021801(R) (2008).
- [22] G. Kulkarni, P. Kumar, and A. K. Jha, Transfer of temporal coherence in parametric down-conversion, *J. Opt. Soc. Am. B* **34**, 1637 (2017).
- [23] G. Kulkarni, V. Subrahmanyam, and A. K. Jha, Intrinsic upper bound on two-qubit polarization entanglement predetermined by pump polarization correlations in parametric down-conversion, *Phys. Rev. A* **93**, 063842 (2016).
- [24] N. Meher, A. S. M. Patoary, G. Kulkarni, and A. K. Jha, Intrinsic degree of coherence of two-qubit states and measures of two-particle quantum correlations, *J. Opt. Soc. Am. B* **37**, 1224 (2020).
- [25] P. Sharma, N. K. Pathak, and B. Kanseri, Controlling polarization entanglement in biphotons generated with partially spatially coherent pump beam, *Results Phys.* **27**, 104506 (2021).
- [26] Y. Ismail, S. Joshi, and F. Petruccione, Polarization-entangled photon generation using partial spatially coherent pump beam, *Sci. Rep.* **7**, 12091 (2017).
- [27] P. G. Kwiat, E. Waks, A. G. White, I. Appelbaum, and P. H. Eberhard, Ultrabright source of polarization-entangled photons, *Phys. Rev. A* **60**, R773 (1999).
- [28] See Supplemental Material at <http://link.aps.org/supplemental/10.1103/PhysRevA.107.L041701> for a detailed derivation of the two-photon density matrix, a detailed derivation of the relative phase, estimation method of the effective angular bandwidth of the pump, and a comparison between theoretical and experimental results for LED-pumped SPDC, including Refs. [22,27,32,33,44–47].
- [29] R. F. Werner, Quantum states with Einstein-Podolsky-Rosen correlations admitting a hidden-variable model, *Phys. Rev. A* **40**, 4277 (1989).
- [30] W. K. Wootters, Entanglement of Formation of an Arbitrary State of Two Qubits, *Phys. Rev. Lett.* **80**, 2245 (1998).
- [31] Y. Nambu, K. Usami, Y. Tsuda, K. Matsumoto, and K. Nakamura, Generation of polarization-entangled photon pairs in a cascade of two type-I crystals pumped by femtosecond pulses, *Phys. Rev. A* **66**, 033816 (2002).

- [32] R. Rangarajan, M. Goggin, and P. Kwiat, Optimizing type-I polarization-entangled photons, *Opt. Express* **17**, 18920 (2009).
- [33] J. B. Altepeter, E. R. Jeffrey, and P. G. Kwiat, Phase-compensated ultra-bright source of entangled photons, *Opt. Express* **13**, 8951 (2005).
- [34] D. F. V. James, P. G. Kwiat, W. J. Munro, and A. G. White, Measurement of qubits, *Phys. Rev. A* **64**, 052312 (2001).
- [35] X. Zhao, L. Ji, D. Liu, Y. Gao, D. Rao, Y. Cui, W. Feng, F. Li, H. Shi, C. Shan, W. Ma, and Z. Sui, Second-harmonic generation of temporally low-coherence light, *APL Photon.* **5**, 091301 (2020).
- [36] W. Zhang, D. Xu, and L. Chen, Polarization entanglement from parametric down-conversion with a LED pump, [arXiv:2211.00841](https://arxiv.org/abs/2211.00841).
- [37] H. Wang, T. Horikiri, and T. Kobayashi, Polarization-entangled mode-locked photons from cavity-enhanced spontaneous parametric down-conversion, *Phys. Rev. A* **70**, 043804 (2004).
- [38] F. Steinlechner, P. Trojek, M. Jofre, H. Weier, D. Perez, T. Jennewein, R. Ursin, J. Rarity, M. W. Mitchell, J. P. Torres, H. Weinfurter, and V. Pruneri, A high-brightness source of polarization-entangled photons optimized for applications in free space, *Opt. Express* **20**, 9640 (2012).
- [39] F. Steinlechner, S. Ramelow, M. Jofre, M. Gilaberte, T. Jennewein, J. P. Torres, M. W. Mitchell, and V. Pruneri, Phase-stable source of polarization-entangled photons in a linear double-pass configuration, *Opt. Express* **21**, 11943 (2013).
- [40] F. Steinlechner, M. Gilaberte, M. Jofre, T. Scheidl, J. P. Torres, V. Pruneri, and R. Ursin, Efficient heralding of polarization-entangled photons from type-0 and type-II spontaneous parametric downconversion in periodically poled KTiOPO_4 , *J. Opt. Soc. Am. B* **31**, 2068 (2014).
- [41] A. Bhattacharjee and A. K. Jha, Experimental demonstration of structural robustness of spatially partially coherent fields in turbulence, *Opt. Lett.* **45**, 4068 (2020).
- [42] Y. Qiu and W. She, The influence of atmospheric turbulence on partially coherent two-photon entangled field, *Appl. Phys. B* **108**, 683 (2012).
- [43] S. P. Phehlukwayo, M. L. Umuhire, Y. Ismail, S. Joshi, and F. Petruccione, Influence of coincidence detection of a biphoton state through free-space atmospheric turbulence using a partially spatially coherent pump, *Phys. Rev. A* **102**, 033732 (2020).
- [44] C. K. Law and J. H. Eberly, Analysis and Interpretation of High Transverse Entanglement in Optical Parametric Down Conversion, *Phys. Rev. Lett.* **92**, 127903 (2004).
- [45] M. P. van Exter, A. Aiello, S. S. R. Oemrawsingh, G. Nienhuis, and J. P. Woerdman, Effect of spatial filtering on the Schmidt decomposition of entangled photons, *Phys. Rev. A* **74**, 012309 (2006).
- [46] S. Castelletto, I. P. Degiovanni, A. Migdall, and M. Ware, On the measurement of two-photon single-mode coupling efficiency in parametric down-conversion photon sources, *New J. Phys.* **6**, 87 (2004).
- [47] B. E. Saleh and M. C. Teich, *Fundamentals of Photonics* (Wiley, New York, 2019).